nature geoscience

LETTERS

PUBLISHED ONLINE: 22 AUGUST 2016 | DOI: 10.1038/NGEO2795

Methane emissions proportional to permafrost carbon thawed in Arctic lakes since the 1950s

Katey Walter Anthony[1]*, Ronald Daanen[2], Peter Anthony[1], Thomas Schneider von Deimling[3,4], Chien-Lu Ping[5], Jeffrey P. Chanton[6] and Guido Grosse[3]

Permafrost thaw exposes previously frozen soil organic matter to microbial decomposition. This process generates methane and carbon dioxide, and thereby fuels a positive feedback process that leads to further warming and thaw[1]. Despite widespread permafrost degradation during the past ~40 years[2–4], the degree to which permafrost thaw may be contributing to a feedback between warming and thaw in recent decades is not well understood. Radiocarbon evidence of modern emissions of ancient permafrost carbon is also sparse[5]. Here we combine radiocarbon dating of lake bubble trace-gas methane (113 measurements) and soil organic carbon (289 measurements) for lakes in Alaska, Canada, Sweden and Siberia with numerical modelling of thaw and remote sensing of thermokarst shore expansion. Methane emissions from thermokarst areas of lakes that have expanded over the past 60 years were directly proportional to the mass of soil carbon inputs to the lakes from the erosion of thawing permafrost. Radiocarbon dating indicates that methane age from lakes is nearly identical to the age of permafrost soil carbon thawing around them. Based on this evidence of landscape-scale permafrost carbon feedback, we estimate that 0.2 to 2.5 Pg permafrost carbon was released as methane and carbon dioxide in thermokarst expansion zones of pan-Arctic lakes during the past 60 years.

Over the last glacial cycle, permafrost soils have accumulated >1,400 Pg of 'old' soil organic carbon (SOC) as the remnants of plants and fauna became sequestered in perennial frozen soils[6–8]. Release of just a fraction of this ancient, frozen carbon pool as carbon dioxide (CO_2) and methane (CH_4) could accelerate future global climate warming (that is, permafrost carbon feedback, PCF) due to the heat-trapping properties of these greenhouse gases[9].

Most PCF studies concern future predictions[8–10]; however, the permafrost carbon pool has already been subject to increased thaw. Observations and modelling show widespread permafrost warming[2–4], near-surface permafrost loss[11], and intense changes in land surface hydrology associated with localized thermokarst activity[12] during the past 40–100 years. Yet no research has quantified old carbon release associated with permafrost thaw during this period.

The potential for old carbon release to the atmosphere as the active layer deepens has been implied from laboratory incubation studies[13–15] and soil warming experiments[13,16]. Several studies reported old permafrost SOC release into aquatic systems from watersheds and coastal erosion[17,18]. Mass balance studies found lower carbon stocks in collapse scars compared to frozen peat plateaux, implying the loss of old carbon[19]. Only one study directly observed old carbon dioxide emission from thermokarst in the unmanipulated upland tundra[5]; there, multiple decades were required for the loss of old SOC to overcome atmospheric carbon uptake from increased plant growth following permafrost thaw. Scientists have concluded that in most terrestrial environments the net movement of old carbon from permafrost to the atmosphere over decades is difficult to detect amidst large input and output fluxes from ecosystem carbon exchange[5,13].

In contrast to terrestrial environments, thermokarst lakes provide a direct conduit for processing and emission of old permafrost carbon to the atmosphere, and these emissions are readily detectable. In ice-rich permafrost regions, permafrost thaw associated with climate warming leads to ground surface collapse and thermokarst-lake formation[20], observed over recent decades[1] and the Holocene epoch[7]. Ancient permafrost soil organic matter (SOM) is largely decomposed deep in anaerobic thaw bulbs (taliks) beneath lakes, where it is not mixed with modern carbon inputs. Due to its low solubility, methane produced from this ancient SOM decomposition is released directly and rapidly to the atmosphere as bubbles[21]. Thus, thermokarst lakes provide a unique setting for demonstrating and quantifying the relationship between permafrost SOC inputs and greenhouse gas release.

Here we used field measurements of lake bubbles and permafrost SOC, radiocarbon dating, remote sensing analysis, and numerical modelling to document the release of old carbon associated with the past 60 years of permafrost thaw surrounding arctic and boreal lakes. Based on the premise that thawed permafrost SOC fuels methane production in thermokarst-affected lakes, we tested three hypotheses: (H1) If the labile fraction of permafrost SOC is limited and becomes depleted over time after thaw, methane emissions from thermokarst expansion zones (lake margins that changed from land to open water during the past 60 years) should exceed emissions from stable open-water zones; (H2) If ebullition (bubbling) in thermokarst expansion zones is produced from permafrost SOC inputs, then methane ebullition in these zones should be proportional to soil carbon erosion rates; (H3) If methane ebullition is produced from soil carbon inputs, then bubble methane radiocarbon ages should reflect the ages of permafrost SOC.

We identified thermokarst expansion zones by overlaying historical (circa 1950s) aerial photos of lakes with present-day shorelines identified in high-resolution satellite imagery (Supplementary Fig. 1). We quantified methane ebullition and radiocarbon ages in 60-year thermokarst expansion zones and stable open-water zones of a variety of lake types in Alaska and Siberia spanning different latitudes (63°–71° N), ecosystems, and

[1]Water and Environmental Research Center, University of Alaska Fairbanks, Fairbanks, Alaska 999775, USA. [2]Division of Geological and Geophysical Surveys, Alaska Department of Natural Resources, Fairbanks, Alaska 999775, USA. [3]Alfred Wegener Institute Helmholtz Centre for Polar and Marine Research, 14473 Potsdam, Germany. [4]Max Planck Institute for Meteorology, 20146 Hamburg, Germany. [5]School of Natural Resources and Extension, University of Alaska Fairbanks, Fairbanks, Alaska 999775, USA. [6]Department of Earth, Ocean and Atmospheric Science, Florida State University, Tallahassee, Florida 32306, USA. *e-mail: kmwalteranthony@alaska.edu

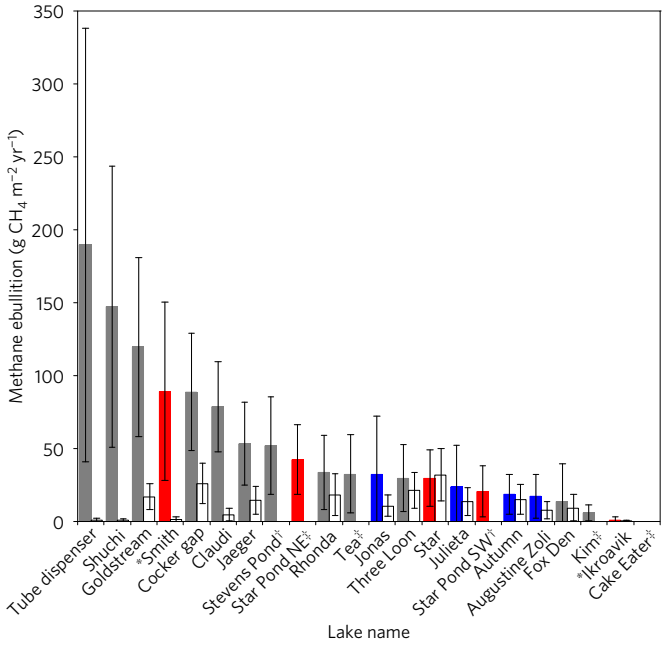

Figure 1 | Methane ebullition in 60-year thermokarst expansion zones (solid bars) and stable open-water zones (non-solid bars) in glacial (blue), yedoma thermokarst (grey) and non-yedoma thermokarst (red) lakes. *Formal lake names (Supplementary Table 1); †Ponds not present on the landscape 60 years ago; ‡No data for stable open-water zones. Standard error bars at the 95% confidence level were calculated by propagating spatiotemporal errors associated with bubble-trap flux measurements and spatial errors associated with ice-bubble surveys.

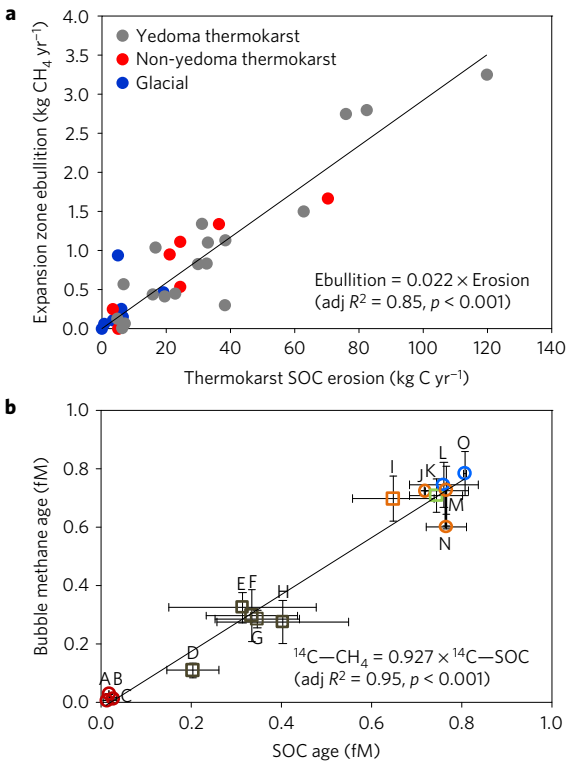

Figure 2 | Relationships between the quantity and age of soil organic carbon (SOC) input to thermokarst-affected lakes and methane emissions from lakes. a, Expansion zone ebullition as a function of thermokarst SOC erosion. **b**, Mean ^{14}C ages of soils (circles) and combined soils and sediments (squares) are expressed as fraction of modern carbon (fM). Points A-O represent class-specific bubbles [1 (red circle), 2 (brown square), 3 (green square), 4 (blue circle) and 5 (orange circle, orange square) (see Methods and Supplementary Fig. 3)] within different regions of Alaska, Canada, Sweden and Siberia. Standard error bars for bubble ($n = 2$–29) and soil profile ($n = 2$–21) means calculated from Supplementary Table 2. Adj; Adjusted.

permafrost types (Supplementary Table 1 and Supplementary Fig. 2, Methods). Additional radiocarbon data were collected for lakes and soils in thermokarst-affected landscapes in Canada and Sweden.

We found that ebullition in the 60-year thermokarst expansion zones in lakes was higher than in stable open-water zones (one-sided Kolmogorov–Smirnov test, $p = 0.0019$) (Fig. 1), indicating that permafrost thaw provides a unique source of SOC to fuel methanogenesis in thermokarst expansion zones (H1; Supplementary Information).

To test H2, we related Geographical Information System (GIS)-based analysis of lake methane ebullition field data collected in ~60 yr thermokarst expansion zones to estimates of SOC mass deposited in these zones as permafrost thawed. SOC erosion was determined by combining field measurements of permafrost SOC stocks adjacent to lakes with numerical modelling of thermokarst subsidence and talik development in these zones (Methods). We found thermokarst-zone methane ebullition to be directly proportional to SOC erosion around lakes, including soils in both the exposed margin bluffs as well as in the radially expanding taliks beneath lakes (Fig. 2a). These results support H2, quantify the relationship between permafrost SOC input to lakes and observed methane emissions, and are evidence of a detectable PCF in present-day ecosystems.

The decadal-scale conversion of thawed permafrost SOC to methane ebullition in our field sites (0.50 ± 0.09 g C-CH_4 kg SOC^{-1} yr^{-1}, mean ± SE, $n = 32$; median 0.37 g C-CH_4 kg SOC^{-1} yr^{-1}) was several orders of magnitude lower than rates derived from lab- and field-based estimates of aerobic-state conversion of thawed permafrost SOC to carbon dioxide (66% and <34%, respectively)[5,17] and ~3-fold lower than the maximum conversion rates of permafrost SOC to methane measured in <1-yr anaerobic laboratory incubations of northern permafrost soils (1.17 g C-CH_4 kg SOC^{-1} yr^{-1}, median)[14]. Lower conversion of SOC to methane in thermokarst zones of arctic lakes compared to anaerobic incubations may be explained by colder mean annual temperature in lake taliks (<1 to 3.5 °C)[22,23] compared to incubations (13 ± 8 °C, mean ± standard deviation, 15 °C median)[14] and by the comparison of decadal-scale average rates in lakes versus short-term maximum rates reported for incubations.

Finally, in our test of H3, we found a strong relationship between the radiocarbon ages of SOC profiles in the regions surrounding lakes and methane-carbon ages in bubbles (Fig. 2b and Supplementary Table 2). Methane in high-flux hotspot seeps located in 60-year thermokarst expansion zones in lakes formed in late Pleistocene-aged yedoma soils (hereafter yedoma lakes) had the oldest ^{14}C ages (32,268 ± 1,295 yr BP; mean ± SE, $n = 21$; max 42,900 yr BP), corresponding to late Pleistocene-aged yedoma SOC thawing deep within taliks (Supplementary Fig. 3). Bubble methane from seeps in other zones of yedoma lakes was also ^{14}C-depleted (11,062 ± 1,160 yr BP, $n = 67$), but the relatively younger methane-carbon age corresponded to sediments of mixed ages eroding from bluffs (older thawed yedoma and younger Holocene-aged SOC), which together form lake sediments overlying taberites (*in-situ* thawed yedoma)[7]. These results are consistent with previous modelling and field studies, which showed the radiocarbon age of methane in yedoma-lake ebullition seeps is oldest along thermokarst margins and decreases in age with distance towards the lake centre[24,25]. Similarly, ebullition methane has more enriched deuterium signatures with increasing distance from the eroding shore[24]. These trends occur

because methane production in the lake centre is disproportionately formed from younger SOM and more modern environmental water once the thawed ancient permafrost substrate has been utilized (H1). Non-seep ebullition bubbles, which are thought to originate from surface lake sediments[21], had the youngest radiocarbon ages in yedoma lakes (2,351 ± 900 yr BP, $n = 8$). These ages were not significantly different from the late Holocene ages observed in seep (2,936 ± 445 yr BP, $n = 11$) and non-seep (2,199 ± 556 yr BP, $n = 6$) bubbles from non-yedoma thermokarst and glacial lakes, indicating that late Holocene-aged permafrost SOC is an important fuel source for bubbles originating from near-surface sediments in all lake types. The nearly 1:1 relationship between radiocarbon ages of soil and methane carbon (Fig. 2b) supports H3, is consistent with previous laboratory incubation studies showing that permafrost contains labile SOC capable of fuelling methanogenesis upon thaw[14,15,22], and demonstrates that thawed permafrost SOC is being converted directly to atmospheric methane.

Most studies of lake area change in the Arctic observe the process of lake expansion during recent decades (Supplementary Table 3). First-order extrapolation of our flux results (Fig. 1) to the extent of 60-year thermokarst expansion in pan-arctic lakes agreed with long-term permafrost carbon mass-balance approaches[7], indicating that the fraction of the terrestrial permafrost carbon pool that has been released as methane from lake-margin thermokarst during the past 60 years is small, probably 0.1–0.3 Pg C-CH_4. Accounting for carbon dioxide, also produced by anaerobic decomposition of thawed permafrost SOM beneath lakes, results in a total permafrost-carbon emission of 0.2–2.5 Pg $C_{(CH4+CO2)}$ from thermokarst expansion zones in pan-arctic lakes during the past 60 years (Supplementary Information and Supplementary Table 5). Palaeoenvironmental records indicate that the PCF from methane associated with thermokarst-lake development was probably larger during the early Holocene[7] (>31 Pg C-CH_4 during 14–8 kyr ago; up to 11 Tg CH_4 yr^{-1} versus ~4 Tg CH_4 yr^{-1} today, Supplementary Information) when higher atmospheric temperatures in the Arctic [1.6 ± 0.8 °C warmer than present during the Holocene Thermal Maximum, 11–9 kyr ago][26] combined with initially less physical protection of permafrost soils by vegetation and lower-relief landscapes[27], culminated in more thermokarst activity than at present[7]. Past and present permafrost soil carbon emissions from terrestrial land surfaces have never been estimated, but the presence of ice-wedge casts south of the modern permafrost boundary[28] is evidence that the permafrost boundary has retreated northwards during the Holocene, implying some additional loss of permafrost carbon from the terrestrial environment.

The PCF has potential to be much larger in the future. PCF models, which largely concern emissions from terrestrial (non-lake) environments[5,9,10], predict release of 12–113 Pg permafrost soil carbon by 2100 under RCP4.5 and RCP8.5 (ref. 10), though additional large emissions may also occur from deep carbon thaw by thermokarst lakes[29] (Fig. 3). These PCF models predict emissions of permafrost soil carbon from thermokarst lakes (103–129 Tg C yr^{-1})[29] and non-lake environments (356–930 Tg C yr^{-1})[10] up to ~100 and ~900 times faster, respectively, during the next 90 years than what has been emitted from thermokarst lakes at any time during the Holocene (1–17 Tg C yr^{-1}; Fig. 3). Large regional temperature increases in the Arctic, up to 7.5 °C by 2100 (Fig. SPM.8, ref. 30), and thicker, organic-rich Holocene-aged deposits subject to thaw and aerobic decomposition as the active layer deepens[6–8] may explain the large divergence between past and near-future permafrost carbon release. Nonetheless, our research indicates that the dramatic increase in permafrost carbon emissions that is expected to imminently occur shows no sign of having commenced (Fig. 3).

In conclusion, this research is the first to show landscape-level conversion of ancient permafrost SOC to old carbon greenhouse gas emissions. Our results indicate that the PCF has been occurring through the release of old carbon from thermokarst expansion of lakes during recent decades. A larger, sustained enhancement of PCF climate warming by 2100 will require far more extensive and intensive thawing of permafrost than what has occurred during the past 60 years (Supplementary Table 5).

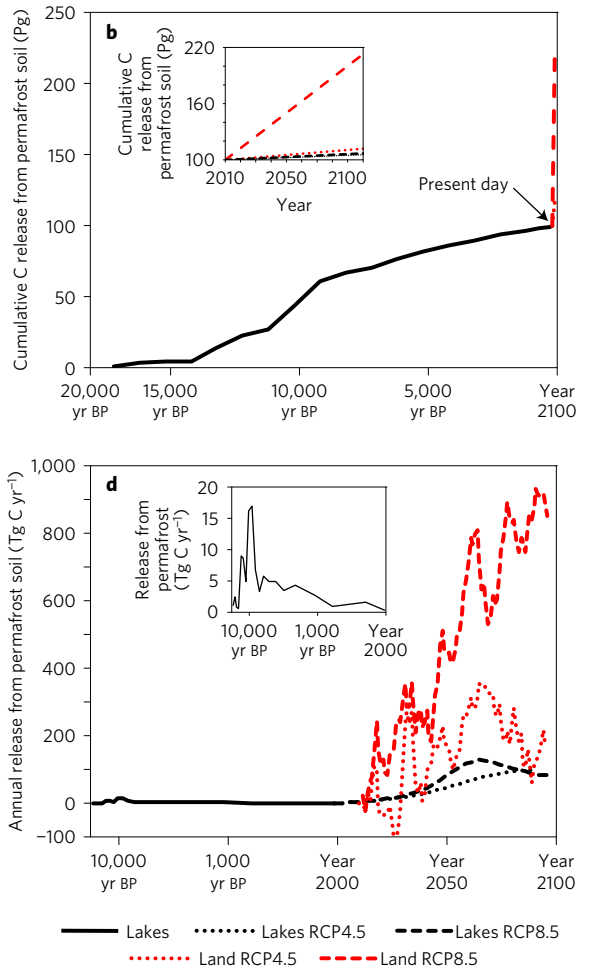

Figure 3 | Modelled emissions of permafrost soil carbon (methane plus carbon dioxide) to the atmosphere during the Holocene and this century. **a**, Emissions during the next 90 years from thermokarst lakes (5.4–6.9 Pg C)[29] and land (12–113 Pg C)[10] could more than double the cumulative lake emission of permafrost-soil carbon since the last deglaciation[7]. **b**, Emissions are shown on a stretched time scale from year 2010 to 2100. **c**, Projected permafrost-soil carbon release during this century from thermokarst lakes[29] and land[10] is shown (note stretched time scale from 2000 to 2100). **d**, Details past yedoma-type thermokarst lake emissions in **c**.

Methods

Methods, including statements of data availability and any associated accession codes and references, are available in the online version of this paper.

Received 5 December 2015; accepted 22 July 2016; published online 22 August 2016

References

1. Walter, K. M., Zimov, S. A., Chanton, J. P., Verbyla, D. & Chapin, F. S. Methane bubbling from Siberian thaw lakes as a positive feedback to climate warming. *Nature* **443,** 71–75 (2006).
2. Romanovsky, V. E. *et al*. Thermal state of permafrost in Russia. *Permafrost Periglac.* **21,** 136–155 (2010).

3. Romanovsky, V., Smith, S. & Christiansen, H. Permafrost thermal state in the polar Northern Hemisphere during the International Polar Year 2007–2009 A synthesis. *Permafrost Periglac.* **21,** 106–116 (2010).
4. Smith, S. *et al*. Thermal state of permafrost in North America: a contribution to the international polar year. *Permafrost Periglac.* **21,** 117–135 (2010).
5. Schuur, E. A. G. *et al*. The effect of permafrost thaw on old carbon release and net carbon exchange from tundra. *Nature* **459,** 556–559 (2009).
6. Hugelius, G. *et al*. Estimated stocks of circumpolar permafrost carbon with quantified uncertainty ranges and identified data gaps. *Biogeosciences* **11,** 6573–6593 (2014).
7. Walter Anthony, K. M. *et al*. A shift of thermokarst lakes from carbon sources to sinks during the Holocene epoch. *Nature* **511,** 452–456 (2014).
8. Schuur, E. A. G. *et al*. Climate change and the permafrost carbon feedback. *Nature* **520,** 171–179 (2015).
9. Schaefer, K., Lantuit, H., Romanovsky, V. E., Schuur, E. A. G. & Witt, R. The impact of the permafrost carbon feedback on global climate. *Environ. Res. Lett.* **9,** 085003 (2014).
10. Koven, C. D. *et al*. A simplified, data-constrained approach to estimate the permafrost carbon–climate feedback. *Phil. Trans. R. Soc. A.* **373,** 20140423 (2015).
11. Lawrence, D. M., Slater, A. G., Romanovsky, V. E. & Nicolsky, D. J. Sensitivity of a model projection of near-surface permafrost degradation to soil column depth and representation of soil organic matter. *J. Geophys. Res. Earth Surf.* **113,** F02011 (2008).
12. Jorgenson, M. T., Shur, Y. L. & Pullman, E. R. Abrupt increase in permafrost degradation in Arctic Alaska. *Geophys. Res. Lett.* **33,** L02503 (2006).
13. Nowinski, N. S., Taneva, L., Trumbore, S. E. & Welker, J. M. Decomposition of old organic matter as a result of deeper active layers in a snow depth manipulation experiment. *Oecologia* **163,** 785–792 (2010).
14. Treat, C. C. *et al*. A pan-Arctic synthesis of CH_4 and CO_2 production from anoxic soil incubations. *Glob. Change Biol.* **21,** 2797–2803 (2015).
15. Drake, T. W., Wickland, K. P., Spencer, R. G. M., McKnight, D. M. & Striegl, R. G. Ancient low-molecular-weight organic acids in permafrost fuel rapid carbon dioxide production upon thaw. *Proc. Natl Acad. Sci. USA* **112,** 13946–13951 (2015).
16. Hicks Pries, C., Schuur, E. A. G., Natali, S. M. & Crummer, K. G. Old soil carbon losses increase with ecosystem respiration in experimentally thawed tundra. *Nat. Clim. Change* **6,** 214–218 (2015).
17. Vonk, J. E. *et al*. Activation of old carbon by erosion of coastal and subsea permafrost in Arctic Siberia. *Nature* **489,** 137–140 (2012).
18. Mann, P. J. *et al*. Utilization of ancient permafrost carbon in headwaters of Arctic fluvial networks. *Nat. Commun.* **6,** 7856 (2015).
19. O'Donnell, J. A. *et al*. The effects of permafrost thaw on soil hydrologic, thermal, and carbon dynamics in an Alaskan peatland. *Ecosystems* **15,** 213–229 (2012).
20. Zimov, S. A. *et al*. North Siberian lakes: a methane source fueled by Pleistocene carbon. *Science* **277,** 800–802 (1997).
21. Walter, K. M., Chanton, J. P., Chapin, F. S., Schuur, E. A. G. & Zimov, S. A. Methane production and bubble emissions from arctic lakes: isotopic implications for source pathways and ages. *J. Geophys. Res. Biogeosci.* **113,** G00A08 (2008).
22. Heslop, J. K. *et al*. Thermokarst-lake methane production potentials along a full talik profile. *Biogeosciences* **12,** 4317–4331 (2015).
23. Tan, Z., Zhuang, Q. & WalterAnthony, K. M. Modeling methane emissions from Arctic lakes: model development and site-level study. *J. Adv. Model. Earth Sy.* **7,** 459–483 (2015).
24. Brosius, L. S. *et al*. Using the deuterium isotope composition of permafrost melt water to constrain thermokarst lake contributions to atmospheric CH_4 during the last deglaciation. *J. Geophys. Res. Biogeosci.* **117,** G01022 (2012).
25. Kessler, M. A., Plug, L. & Walter Anthony, K. Simulating the decadal to millennial scale dynamics of morphology and sequestered carbon mobilization of two thermokarst lakes in N. W. Alaska. *J. Geophys. Res. Biogeosci.* **117,** G00M06 (2012).
26. Kaufman, D. *et al*. Holocene thermal maximum in the western Arctic (0–180° W). *Quat. Sci. Rev.* **23,** 529–560 (2004).
27. Jorgenson, M. T. *et al*. Reorganization of vegetation, hydrology and soil carbon after permafrost degradation across heterogeneous boreal landscapes. *Environ. Res. Lett.* **8,** 035017 (2013).
28. Vandenberghe, J. *et al*. The Last Permafrost Maximum (LPM) map of the Northern Hemisphere: permafrost extent and mean annual air temperatures, 25–17 ka BP. *Boreas* **43,** 652–666 (2014).
29. Schneider von Deimling, T. *et al*. Observation-based modelling of permafrost carbon fluxes with accounting for deep carbon deposits and thermokarst activity. *Biogeosciences* **12,** 3469–3488 (2015).
30. IPCC *Summary for Policymakers in Climate Change 2013: The Physical Science Basis* (eds Stocker, T. F. *et al*.) (Cambridge Univ. Press, 2014).

Acknowledgements

We thank B. Jones at the USGS for contributions to remote sensing data sets and for providing valuable comments on the manuscript, C. Koven for model data contributions in Fig. 3, and Ted Schuur for assistance with AMS radiocarbon dating. This work was supported by the NSF ARC-1304823, NASA ABoVE NNX15AU49A, NSF OPP-1107892, NSF ARCSS 1500931, USDA-Hatch, US Department of Energy DESC0010580 and ERC.

Author contributions

K.W.A. conceived of the study and wrote the paper. K.W.A., P.A., C.-L.P. and G.G. conducted field and lab work. R.D. and T.S.v.D. performed numerical modelling. Isotopic analyses were conducted in the laboratory of J.P.C. All authors commented on the analysis, interpretation and presentation of the data, and were involved in the writing.

Additional information

Supplementary information is available in the online version of the paper. Reprints and permissions information is available online at www.nature.com/reprints. Correspondence and requests for materials should be addressed to K.W.A.

Competing financial interests

The authors declare no competing financial interests.

Methods

Methane sampling and analyses. We sampled methane from 37 lakes in Alaska, Siberia and Sweden that differed according to latitude, ecozone, permafrost soil carbon stocks and thermokarst margin expansion rates during recent decades. Supplementary Table 1 provides metadata for these lakes plus two additional Canadian lakes from which we included literature-sourced data in our analysis. Lakes were classified as: yedoma lakes (that is, thermokarst lakes formed by thaw Pleistocene-aged, ice-rich, syngenetic, silt-dominated yedoma permafrost)[20,31]; non-yedoma thermokarst lakes formed by thawing of icy, organic-rich permafrost soils outside the Yedoma region[32]; and glacially formed lakes in permafrost-dominated regions[33]. Although glacial lakes did not originate by thermokarst processes, their shores are often subject to thermokarst expansion today due to the thaw of surrounding ice-rich ground.

Methane sampling in lakes consisted of quantifying ebullition flux (see section 'Field measurements of methane ebullition flux.') using ice-bubble surveys coupled to bubble trap measurements in ~60-year thermokarst expansion zones and non-thermokarst zones. The latter included littoral and profundal lake areas that remained stable open-water surfaces during the past 60 years. To estimate the magnitude of old methane ebullition we measured bubble methane concentrations, stable isotopes and radiocarbon ages (see section 'Methane concentration and radiocarbon age.').

Field measurements of methane ebullition flux. Methane readily forms bubbles in lake sediments. Newly formed bubbles follow existing escape pathways through sediments[34], resulting in point sources of continuous ebullition seepage at the sediment-water interface. During the ice-free season, bubbles rise through the water column and escape to the atmosphere. In winter, surface lake ice seasonally traps seep bubbles, although the majority of winter-bubble methane escapes lakes in spring as ice melts[35]. We estimated ebullition from lake sediments associated with discrete seeps following the lake-ice ebullition survey method of Walter Anthony and colleagues[36]. Seeps were identified as A, B, C, and Hotspot types according to patterns of bubbles trapped in early winter lake ice. The lake ebullition seep-classification system has been described in detail in previous publications[1,36,37]. Briefly, A-type ebullition seeps are relatively small clusters of ebullition bubbles in which individual bubbles stack on top of each other in the winter ice sheet without merging laterally. Due to progressively higher ebullition rates, individual bubbles of B-type seeps laterally merge into larger bubbles under the ice before freezing in ice. Seeps of Type A and Type B produce low-gas-volume clusters of bubbles in lake ice with cluster diameters typically <40 cm. The larger Type C seeps result in large (usually >40 cm diameter) gas pockets in ice separated vertically by ice layers containing few or no bubbles. Bubble-trap measurements showed that the solid ice layers in between the large gas pockets of Type C seeps represent periods of relative quiescence between large ebullition events[21,36]. Hotspot seeps have the greatest mean daily bubbling rates. The frequency of ebullition release from hotspot seeps and the associated water column convection created by rising bubble plumes maintains mostly ice-free holes in winter lakes[35,38].

We removed snow from early winter lake ice to expose ebullition bubble clusters trapped in ice for seep classification. We quantified seep density, GPS-mapped seeps, and measured fluxes and collected gas using submerged bubble traps. On foot, we surveyed 9,102 individual seeps within 135 plots (30–640 m^2 per plot, average of six plots per lake). Ice-bubble survey plots were typically 1-m-wide transects originating from thermokarst and non-thermokarst margins, oriented perpendicular to the shores and extending towards the lake centre. Additional lake-centre transects were also surveyed. We calculated seep density within thermokarst and non-thermokarst zones as the total number of seeps surveyed within each zone divided by area surveyed.

To convert seep densities to estimates of annual volumetric ebullition we measured ebullition fluxes year-round using submerged bubble traps. In some lakes, ice was opened above the seeps for placement of submerged bubble traps over the seeps in winter. Semi-automated bubble traps remained in place over individual seeps year-round[36], providing daily and seasonal bubbling rates for individual seeps. Fluxes from other seeps were measured over the short term (<6 days) using manual bubble traps. Altogether the seep flux data set consists of ~210,000 individual flux measurements made using submerged bubble traps placed over ebullition seeps year-round. Seep-class-specific flux rates measured on a subset of seeps were applied to all mapped seeps to estimate whole-lake ebullition rates. In a recent comparison of methods, Walter Anthony and Anthony[37] showed that when at least three 50-m transects per lake are used to quantify seep ebullition, the estimate of mean whole-lake ebullition is 4–5 times more accurate than the mean flux determined by placement of ~twenty 0.2-m^2 bubble traps randomly distributed across lake surfaces.

Uncertainties associated with our ebullition estimates were calculated by propagating spatial errors associated with ice-bubble surveys, which are a function of survey area and ebullition seep density[37], and spatiotemporal errors associated seep-class-specific bubble-trap flux measurements.

Methane concentration and radiocarbon age. To determine mass-based estimates of methane ebullition, we applied lake-specific measurements of bubble methane concentrations to the individual lakes where seep-bubble gases were collected and measured, following methods detailed by Walter and colleagues[21]. Briefly, gases were collected from submerged bubble traps into 60-ml glass serum vials, sealed with butyl rubber stoppers, and stored under refrigeration in the dark until laboratory analyses. We measured bubble methane and carbon dioxide concentrations using a using a GC-2014 gas chromatograph (Shimadzu) equipped with a flame ionization detector and a PLOT alumina column (detector temperature 250 °C, oven 40 °C, high-purity helium as carrier gas) at the University of Alaska Fairbanks. Up to 246 individual seep ebullition events were measured per lake. In lakes where few or no seep-bubble gas concentrations were determined, we applied mean values of methane concentration by seep class from all study lakes[36]: A, 73% CH_4; B, 75% CH_4; C, 76% CH_4; Hotspot 78% CH_4. Carbon dioxide concentration in seep ebullition bubbles was 0.53 ± 0.44% by volume (mean ± standard deviation).

In addition to bubble gas from seeps, we also collected ebullition gas from traps placed randomly in lakes, termed 'Background ebullition'. Spatial analysis showed that random placement of traps is unlikely to capture seep ebullition in these lakes due to the point-process characteristic of seep bubbling[1,37] (that is, points occupy a relatively small fraction of lake area, even if they are large in number). In two lakes, surface sediments were stirred to collect gas bubbles; stirred bubbles did not represent natural ebullition events.

We determined the radiocarbon age of methane in lake bubbles collected from seeps, background bubble traps and stirred sediments. In total 105 ebullition events and four stirred bubble samples collected from 24 were dated. Subsamples of bubbles were purified and combusted on a helium gas stream, as described in Chanton and colleagues[39]. Carbon dioxide in the samples was removed in a pre-combustion trap placed in liquid nitrogen. Methane was then combusted to carbon dioxide by passing it over copper oxide at 800 °C. Prior to this, the copper oxide was charged with oxygen at 600 °C overnight. Following combustion, water was removed in pentane-liquid nitrogen slush, and the carbon dioxide was then trapped in a liquid nitrogen trap. Carbon dioxide was then purified by running it though another water trap; its volume was measured in a pressure manometer; and it was then sealed in a 6 mm Pyrex tube. Samples were then catalytically reduced to graphite[40], and the $^{14}C/^{12}C$ isotopic ratios were measured by accelerator mass spectrometry at the Woods Hole Oceanographic Institution's National Ocean Sciences AMS (NOSAMS) Facility and the Keck Carbon Cycle AMS Facility at the University of California, Irvine. Samples of ^{14}C dead tank methane were prepared and analysed, as were samples yielding a result of 0.004 ± 0.0009 fraction modern carbon ($n = 8$).

To assess the relationship between radiocarbon ages of methane in ebullition bubbles and SOC ages (H3), we first classified bubbles according to ebullition type, zone of lake in which bubbles were collected, and lake type (Supplementary Fig. 3). The average radiocarbon age of SOC in soil profiles for each region was summarized from our field data and the literature (Supplementary Table 2). Radiocarbon results are reported as conventional radiocarbon ages (years before present, yr BP) and as the fraction of modern carbon (fM). The relationship between these units is expressed as Age = −8033× ln(fM). All averaging of radiocarbon data was performed on ^{14}C activity expressed as fM.

Soils sampling and analyses. We sampled soil profiles adjacent to lakes in late summer 2008 and 2010 by digging soil pits for sampling active layer soils and using a modified SIPRE drill (Jon Holmgren's Machine Shop, Fairbanks) to obtain underlying permafrost soil samples up to 3.7 m deep. We also sampled permafrost soils to 5.6 m depth in vertical exposures in the regions of our study lakes. At exposure sites we removed seasonally thawed soils to expose permafrost in cross section along vertical profiles before sampling with a 75-cm^3 hole-saw mounted on a portable drill. We studied exposures with the steepest bluff angles to avoid locations with thawed, slumped, and re-frozen soil material. At most sites we sampled known volumes of soils for bulk density determination; however, in some yedoma profiles on the northern Seward Peninsula where we lacked volumetric data, we calculated bulk density values based on larger regional yedoma data sets[41]. We classified soils in the field according to Soil Survey Staff[42] and Ping[43]. We determined the gravimetric moisture content of thawed, active layer soil samples as weight loss dried at 105 °C, expressed as percentage of wet weight. We estimated gravimetric ice content of permafrost samples using the same method. We determined organic and inorganic matter contents, after oven drying, by loss-on-ignition (LOI) at 550 °C and 950 °C for two hours, respectively[44]. Since the majority of our study sites were in Alaska, we estimated organic carbon concentrations in samples based on the relationship between LOI (percentage organic matter, P_{om}) and organic carbon concentration (P_{oc}): $P_{OC} = 0.527 * P_{OM}$ ($p < 0.0001$; $r^2 = 0.990$) determined from 421 arctic and boreal Alaska sites[45]. This is similar to the mean peat carbon content across western Canada (0.52 g C g OM^{-1})[46] and Siberia (0.55 g C g OM^{-1})[7]. The organic carbon density (kg C m^{-3}) was calculated as dry bulk density multiplied by percentage organic carbon on a per sample basis. At some sites, plant macrofossils were selected from

the soil profiles for ^{14}C AMS dating at the W. M. Keck Carbon Cycle AMS Laboratory or at the NOSAMS Facility. In addition to collecting our own data, we synthesized data derived from published literature and databases for Alaska and northeast Siberia soil carbon stocks[22,47–49], stratigraphy, and ^{14}C ages (Supplementary Table 2).

Spatial analysis. We used a geospatial analysis approach combined with numerical modelling of permafrost thaw to relate methane ebullition fluxes to soil carbon inputs in zones of lakes that changed from land to water via thermokarst expansion during the past ~60 years. Black and white aerial photos from circa 1950 were acquired from the USGS EROS Data Center. We also acquired high-resolution panchromatic satellite imagery for our study sites from circa 2010 from the Digital Globe family of satellites. All imagery used has nominal resolutions of ≤1 m. For each site, the aerial imagery was georeferenced to a recent satellite image, which served as base imagery. Study lakes were then manually mapped in ArcGIS as polygon shapefiles.

For each lake shapefile, polygons of the historic and current lake perimeters were overlaid in ArcGIS 9.3 (ESRI). The historic lake polygon was clipped from the current lake polygon to identify and quantify the area of thermokarst lake expansion during the intervening time period. While all of the imagery was acquired during the same season (July or August), differences between wet and dry years may also impact measurements of lake surface area. However, we felt that the comparisons between the two time slices were relevant due to the same target season, the very high image resolution, and the established methodology used to delineate water bodies and shoreline change[50]. Moreover, the spatial characteristics of our lake expansion observations suggest that seasonal or inter-annual effects from variable water levels are of low relevance. In most of our study lakes we observed expansion in some areas of the shoreline and shrinkage and/or no change in other areas of the shoreline of the same lakes (Supplementary Fig. 1). This observation of multidirectional change of shorelines within individual lakes supports the assumption that detected expansion along shorelines over ~60 yr reflects actual and lasting transition from land surface to lake. In addition, many of the yedoma and kettle lakes we studied had steep margins (usually >0.5 m to ~12 m bluff heights) and/or had outlet streams—characteristics which limit the impact of water level fluctuations on the surface area measurements. Our analysis did not include floodplain lakes, which often are more variable in their surface area due to seasonal or interannual water level changes depending on spring floods and the degree of fluvial connectivity[51].

In ArcGIS we intersected thermokarst lake expansion polygons with ebullition survey polygons to determine the portion of methane survey data that fell within the zone of lake expansion. Mean annual ebullition rates for all seeps located within the thermokarst expansion zone were summed to determine total annual seep ebullition within this zone. Linear lake expansion was determined manually using the ArcMap measure tool, snapping to lake shorelines, and measuring perpendicularly from historic to current shorelines in the location of methane survey transects.

Modelling permafrost SOC release into lakes. We calculated the volume of permafrost soil that thawed and eroded into lakes during the ~60 yr observation period using lake bathymetric field measurements and a cubic curve fitting method of the lake bottom profile between observations from the shore to lake centre, which is related to the thaw bulb depth using the excess ice content in permafrost. This section details this numerical modelling approach and its underlying assumptions.

Thermokarst-lake expansion results from thermal erosion of permafrost soils along lake shores. Subsidence is the direct result of excess ground ice melt. This loss of ice means loss in soil volume and a loss in soil stability. Thawed soils slump into the voids left behind by the melting excess ice, thus lowering the overall surface elevation of the shoreline.

Building on existing talik modelling efforts[25,52], we calculated the volume of permafrost soils that thawed and eroded into lakes during the ~60 yr observation period using an iterative cubic curve fitting method of the talik profile from the thermokarst lake shore to the centre of the lake. Lake-specific input to the talik profiling model included: shoreline positions of lakes ~60 years ago, determined from remote sensing imagery; time between remote sensing observations of shoreline positions ~60 years ago and during 2009–2010; average lake expansion rates for the ~60 year study calculated by combining the previous two factors using GIS data analysis; present-day lake water depth at the point where the shoreline was ~60 years ago determined by field measurements; and volumetric ice content of permafrost surrounding lakes determined from past regional studies[41,52–59]. At select locations we measured active layer depth at the present-day shoreline using an active layer probe; we assumed these values are representative for other similar lake sites. Maximum lake depth was measured with through-ice sonar bathymetric surveys in early winter using a Depthmate model SM5 portable sounder (Laylin Associates LTD) or from a boat during the open-water season using a sidescan sonar system (Humminbird 798ci HD SI Combo). Distance from the thermokarst shore to the lake centre was determined from very high resolution remote sensing data (historic aerial images, recent satellite images) in ArcGIS.

We fit a cubic equation to three points of the lake bottom bathymetry using an iterative method and the simplified assumption that water elevation remained constant during ~60 years. The three points consisted of water depth at the lake shore, which was by definition zero; present-day lake water depth at the point where the shoreline was ~60 years ago; and water depth in the lake centre. Lake depth ld is given by equation (1) as a function of shore distance,

$$ld = a \times D^3 + b \times D^2 + c \times D + d \quad (1)$$

where a, b, c and d are fitting parameters, and D is the distance from the shore. c and d are assumed 0, while parameters a and b are fitted to measurements. By moving the cubic curve along the radius of the lake outwards in yearly time steps we estimated the water depth between the current and the former shoreline by year. The difference between the two cubic lines representing two consecutive years is the added amount of water to the lake due to thermokarst expansion each year. To convert the water depth to sediment thaw depth, we use the permafrost ice content estimate for the region surrounding the lake. We assumed that the thickness increase of the water depth is approximately the same as the amount of ice lost from the ground. The volume arising from the density difference between water and ice is assumed to be the same volume that is added to the lake by suspended sediments over that same period. Most shoreline degradation occurs in the latter part of summer after the active layer has thawed and when ice-rich permafrost starts thawing. Assuming that the active layer is a fixed thickness layer that becomes part of the lake sediment, we calculated the volume of sediment (formerly permafrost SOC from our data and the literature)[22,47–49] that entered into the lake due to permafrost degradation. In our model, this sediment, with organic matter contents determined from SOC stocks adjusted for volumetric ice content, makes up the talik or thawed sediment exposed to microbial decomposition and methane production.

Statistics. To test the relationships between SOC erosion and expansion zone ebullition, and between SOC age (fM) and bubble methane age (fM), we used linear regression. The data met standard criteria for regression analysis. In testing the second relationship, weighted regression was used to account for non-constant variance. The one-sided Kolmogorov Smirnov test was used to test differences among non-normally distributed data sets. Statistical analyses were performed using the R package[60].

Data availability. The authors declare that the study lake metadata, pan-arctic lake change data, and radiocarbon methane and soil organic carbon data supporting the findings of this study are available within the article's Supplementary Information files. All other data that support the findings of this study are available from the corresponding author upon request.

References

31. Murton, J. B. *et al*. Palaeoenvironmental interpretation of Yedoma Silt (Ice Complex) deposition as Cold-Climate Loess, Duvanny Yar, Northeast Siberia. *Permafrost Periglac.* **26,** 208–288 (2015).
32. Grosse, G., Jones, B. & Arp, C. in *Treatise on Geomorphology* Vol. 8 (ed. Shroder, J. F.) 325–353 (Academic, 2013).
33. Wik, M., Varner, R., Walter Anthony, K., MacIntyre, S. & Bastviken, D. Climate-sensitive northern lakes and ponds are critical components of methane release. *Nat. Geosci.* **9,** 99–105 (2016).
34. Scandella, B. P., Varadharajan, C., Hemond, H. F., Ruppel, C. & Juanes, R. A conduit dilation model of methane venting from lake sediments. *Geophys. Res. Lett.* **38,** L06408 (2011).
35. Greene, S., Walter Anthony, K. M., Archer, D., Sepulveda-Jauregui, A. & Martinez-Cruz, K. Modeling the impediment of methane ebullition bubbles by seasonal lake ice. *Biogeosciences* **11,** 6791–6811 (2014).
36. Walter Anthony, K. M. *et al*. Estimating methane emissions from northern lakes using ice bubble surveys. *Limnol. Oceanogr. Meth.* **8,** 592–609 (2010).
37. Walter Anthony, K. M. & Anthony, P. Constraining spatial variability of methane ebullition seeps in thermokarst lakes using point process models. *J. Geophys. Res. Biogeosci.* **118,** 1015–1034 (2013).
38. Zimov, S. A. *et al*. in *Permafrost Response on Economic Development, Environmental Security and Natural Resources* (eds Paepe, R. & Melnikov, V. P.) 511–524 (NATO Science Series 2, 76, Kluwer Academic, 2001).
39. Chanton, J. P. *et al*. Radiocarbon evidence for the importance of surface vegetation on fermentation and methanogenesis in contrasting types of boreal peatlands. *Glob. Biogeochem. Cy* **22,** GB4022 (2008).
40. Vogel, J. S., Turteltaub, K. W., Finkel, R. & Nelson, D. E. Accelerator mass spectrometry. *Anal. Chem.* **67,** 353A–359A (1995).
41. Strauss, J. *et al*. The deep permafrost carbon pool of the Yedoma region in Siberia and Alaska. *Geophys. Res. Lett.* **40,** 6165–6170 (2013).

42. Soil Survey Staff *Keys to Soil Taxonomy* 10th edn USDA-Natural Resources Conservation Service (USDA-Natural Resources Conservation Service, 2016).
43. Ping, C. L. Gelisols: Part II. Classification and related issues. *Soil Horiz.* **54,** http://dx.doi.org/10.2136/sh2013-54-4-gc (2013).
44. Dean, W. E. Determination of carbonate and organic matter in calcareous sediments and sedimentary rocks by loss on ignition: comparison with other methods. *J. Sed. Petr.* **44,** 242–248 (1974).
45. Michaelson, G. J., Ping, C. L. & Clark, M. H. Soil pedon carbon and nitrogen data for Alaska: an analysis and update. *Open J. Soil Sci.* **3,** 132–142 (2013).
46. Bauer, I. E., Bhatti, J. S., Cash, K. J. & Tarnocai, C. Developing statistical models to estimate the carbon density of organic soils. *Can. J. Soil Sci.* **86,** 295–304 (2006).
47. Hamilton, T. D., Craig, J. L. & Sellmann, P. V. The Fox permafrost tunnel "A late Quaternary geologic record in central Alaska". *Geol. Soc. Am. Bull.* **100,** 948–969 (1988).
48. Harden, J. W. *et al*. Field information links permafrost carbon to physical vulnerabilities of thawing. *Geophys. Res. Lett.* **39,** L15704 (2012).
49. Hugelius, G. *et al*. The Northern Circumpolar Soil Carbon Database: spatially distributed datasets of soil coverage and soil carbon storage in the northern permafrost regions. *Earth Syst. Sci. Data* **5,** 3–13 (2013).
50. Jones, B. M. *et al*. Modern thermokarst lake dynamics in the continuous permafrost zone, northern Seward Peninsula, Alaska. *J. Geophys. Res. Biogeosci.* **116,** G00M03 (2011).
51. Tarasenko, T. V. Interannual variations in the areas of Thermokarst lakes in Central Yakutia. *Water Res.* **40,** 111–119 (2013).
52. West, J. J. & Plug, L. J. Time-dependent morphology of thaw lakes and taliks in deep and shallow ground ice. *J. Geophys. Res. Earth Surf.* **113,** F01009 (2008).
53. Rampton, V. N. in *Research in Polar and Alpine Geomorphology. Third Guelph Symposium on Geomorphology 1973* (eds Fahey, B. & Thompson, R. D.) 43–59 (1974).
54. Bockheim, J. G., Everett, L. R., Hinkel, K. M., Nelson, F. E. & Brown, J. Soil organic carbon storage and distribution in arctic tundra, Barrow, Alaska. *Soil Sci. Soc. Am. J.* **63,** 934–940 (1999).
55. Jorgenson, T. *et al*. *Permafrost characteristics of Alaska* In *Proc. 9th Int. Conf. Permafrost map in scale 1:7,000,000* (eds Kane, D. L. & Hinkel, K. M.) (Institute of Northern Engineering, 2008).
56. Kanevskiy, M., Shur, Y., Fortier, D., Jorgenson, M. T. & Stephani, E. Cryostratigraphy of late Pleistocene syngenetic permafrost (yedoma) in northern Alaska, Itkillik River exposure. *Quat. Res.* **75,** 584–596 (2011).
57. Kanevskiy, M., Dillon, M., Stephani, E. & O'Donnell, J. In *Proc. 10th Int. Conf. Permafrost* 191–196 (2012).
58. Kanevskiy, M. *et al*. Cryostratigraphy and permafrost evolution in the lacustrine Lowlands of West-Central Alaska. *Permafrost Periglac.* **25,** 14–34 (2014).
59. Ulrich, M., Grosse, G., Strauss, J. & Schirrmeister, L. Quantifying wedge-ice volumes in yedoma and thermokarst basin deposits. *Permafrost Periglac.* **25,** 151–161 (2014).
60. Development Core Team *R: A Language and Environment for Statistical Computing* (R Foundation for Statistical Computing, 2009); http://www.R-project.org